Irreversibility analysis of a thermally driven flow of a water-based suspension with dispersed nano-sized capsules of phase change material

Seyed Mohsen Hashem Zadeh[1], S.A.M. Mehryan[2], Mohammad Saidul Islam[3], Mohammad Ghalambaz[4,5,*]

[1]Department of Mechanical Engineering, Shahid Chamran University of Ahvaz, Iran.

[2]Young Researchers and Elite Club, Yasooj Branch, Islamic Azad University, Yasooj, Iran.

[3]School of Mechanical and Mechatronic Engineering, Faculty of Engineering and Information Technology, University of Technology Sydney, Ultimo, NSW 2007, Australia.

[4] Metamaterials for Mechanical, Biomechanical and Multiphysical Applications Research Group, Ton Duc Thang University, Ho Chi Minh City, Vietnam.

[5]Faculty of Applied Sciences, Ton Duc Thang University, Ho Chi Minh City, Vietnam.

*Corresponding author: M. Ghalambaz (mohammad.ghalambaz@tdtu.edu.vn)

Abstract

A precise understanding of the thermal behaviour and entropy generation of a suspension comprising nano-encapsulated phase change materials (NEPCM) is important for the thermal energy storage and heat transfer enhancement in various engineering applications. Studies to date, have improved the knowledge of the heat transfer of NCPCM. However, a suspension comprising NEPCM in the porous medium could enhance the overall heat transfer performance. Therefore, this study aims to investigate the thermal, hydrodynamic and entropy generation behaviour of the NEPCM-suspensions in a porous medium. Conjugate natural convection heat transfer and entropy generation in a square cavity composed of a porous matrix (glass balls), occupied by a suspension comprising nano-encapsulated phase change materials, and

two solid blocks is numerically investigated. Galerkin Finite Element Method is employed to solve the nonlinear coupled equations for the porous flow and heat transfer. The phase transition and the released/absorbed latent heat of the nano-capsules are attributed in a temperature-dependent heat capacity field. The thermal conductivity ratio ($1 \leq R_k \leq 100$), the Darcy number ($10^{-5} \leq Da \leq 10^{-1}$), the Stefan number ($0.2 \leq Ste \leq 1$), the porosity of porous medium ($0.2 \leq \varepsilon \leq 0.9$), the dimensionless fusion temperature ($0.05 \leq T_{fu} \leq 0.95$), the solid walls thickness (d_s = 0.1 and 0.3), and the volume fraction of the nano-capsules ($0.0 \leq \varphi \leq 5\%$) are considered for the numerical calculations. The numerical results illustrate that the rates of heat transfer and the average Bejan number are maximum and the generated entropy is minimum when the fusion temperature of the nano-capsules is T_{fu} = 0.5. Besides, adding the nano-sized particles of encapsulated phase change materials to the host fluid increases the heat transfer rate up to 45% (for the studied set of parameters) and also augments the average Bejan number. The total entropy generation elevates with the increment of the volume fraction of the nanoparticles, for low values of the Darcy number; however, a downward trend can be found for higher values of the *Da*. The combination of NEPCM-suspensions (with latent heat thermal energy storage) and a porous medium (with the extended surface area) provides an extensive capability for thermal enhancement and energy storage applications. In this regard, the findings of the current work demonstrate that the selection of the fusion temperature and Darcy number are two essential key parameters, which could change the trend of the results.

Keywords: Entropy generation; Porous medium; Melting temperature; Phase change heat transfer; Nano-Encapsulated Phase Change Materials; Stefan number.

.

Nomenclature

Latin symbols	
Be	Bejan number
C_p	Specific heat of the suspension in constant pressure
Cr	Suspension heat capacity ratio
d	Width of the solid rectangular blocks
Da	Darcy number
f	Dimensionless phase transient function
g	Acceleration of gravity
h_{sf}	
k	Thermal conductivity coefficient
L	Height of the enclosure, the characteristic length
Nc	Conductivity number of nanoliquid
Nu	Nusselt number
Nv	Dynamic viscosity number of nanoliquid
p	Dimensional form of the pressure field
P	Non-dimensional form of the pressure field
Q	Energy transfer from the hot element
Pr	Prandtl number
Ra	Rayleigh number
R_k	Thermal conductivity ratio
S_{gen}	Total entropy generation
S_{Th}	Heat transfer component of the entropy generation
$S_{Viscous}$	Fluid friction component of the entropy generation
Ste	Stefan number
T	Temperature
T_{fu}	Fusion temperature of the core of the nano-capsules
T_{Mr}	Melting temperature range
u	x-component of the velocity
v	y- component of the velocity
x	x-Cartesian coordinate
y	y-Cartesian coordinate
Greek symbols	
ε	Porosity of the solid matrix
μ	Dynamic viscosity
α	Coefficient of thermal diffusivity
β	Coefficient of thermal expansion
δ	Melting temperature window in the non-dimensional form
ξ	Heat capacity of the nano-capsules to water

ρ	Density
φ	Nano-capsules' volume fraction in water
Θ	Irreversibility parameter
Ψ	Stream-function
η	Mass ratio of the core to the shell
Superscript	
*	Dimensional parameters
Subscript	
avg	Averaged value
b	Bulk properties
co	Properties of the core of the nano-capsules
eff	Effective value
f	Water
h	Hot surface
t	Total
p	Nanoparticles containing phase change material
s	Porous medium
sh	Properties of the shell of the nano-capsules
w	Wall

1. Introduction

Thermal energy storage and heat transfer enhancement attracted the interest of the researchers in different engineering applications due to the increasing demand for energy in real life. In reality, thermal energy loss in various engineering systems is significant as most of the systems are not completely thermodynamically efficient. Various techniques like solar energy storage [1], cryogenic energy storage [2], and heat pump storage [3] are used to store the energy from different sources. In recent years, researchers have employed phase change materials (PCM) with the existing system to store and transfer the thermal energy as PCM can store a significant amount of energy. It is evident that PCM can store about 5 to 14 time's higher energy than conventional storage materials [4]. Despite the high-storage capacity, PCM can transfer a low amount of heat to the surroundings, while engineering applications need higher heat transfer [5].

The available literature uses various porous media [6, 7], shape-specific finned surface [8], and encapsulation techniques [9] to enhance the heat transfer efficiency of the stored energy in PCM. Composites of metallic foam/PCM (CPCMs) are shown to have significant advantages in terms of overall thermal conductivity [10, 11], melting front velocity [12], or stored energy [13]. For instance, Xiao et al. [10] analyzed paraffin/nickel foam and paraffin/copper foam composite phase change materials in a Latent Heat Thermal Storage System and revealed that the thermal conductivity of the composite could be elevated up to fifteen times higher than the case of pure PCM. Mancin et al. [14] surveyed the phase change process of three different paraffin-waxes in copper foam. They demonstrated the high capability of the metallic foams for increasing heat transfer in passive systems.

The porous and shape-specific finned surfaces influence the flow field and extend the heat transfer surface area, which leads to the overall heat transfer enhancement. On the contrary, encapsulation is the technique, which coats a PCM material and prevents is from any reaction with the fluid or solid phase of the system during thermal heat absorption. Encapsulation influences the overall heat transfer by increasing the heat transfer surface area and thermal stability of the PCM. The available literature classified the PCM encapsulation in three different categories macro (>1mm), micro (1-1000μm) and nano (1-1000nm) [4]. A wide range of studies has analyzed the macro [9, 15, 16] and micro-encapsulation [17, 18] of PCM materials for thermal heat storage and heat transfer purpose. Most of those studies have reported that micro-encapsulated PCM provides higher heat transfer than the microencapsulated PCM.

In the micro-encapsulated system, melting and solidification of the PCM happen quicker than the macro-encapsulated system, which eventually increases the overall heat transfer in micro-encapsulated PCM [19]. However, nano-encapsulated PCM could boost the overall heat transfer due to its large surface area, tiny size, thermal and mechanical stability [20]. Studies over the past few decades tried to improve the heat transfer efficiency and analyzed the suspension of the nanoparticles without considering the phase change of the material.

Several numerical and experimental studies calculated the heat transfer of nano-capsulated PCMs in various systems. A numerical study analyzed the heat transfer in a micro-tube heat sink by considering the phase change of the nano-encapsulated PCMs and reported a significant increase in the thermal performance of the heat sink [21]. A finite volume based study illustrated the thermal performance of the nano-encapsulated PCM in an unconfined cylinder [22]. The study concluded that dispersing a higher volume concentration of the particles enhanced the thermal performance. An experimental study examined the thermal performance of a mini channel heat sink [23] and found that the flow rate and particle volume fraction influence the overall heat transfer.

Almost all of the heat transfer studies regarding the nano-encapsulated PCM focused on forced convection heat transfer. Recently, Ghalambaz et al. [24] performed a comprehensive analysis of the free convection thermal enhancement of nano-encapsulated PCMs in a square cavity. The study used insulated top and bottom walls, while the left wall of the model was considered hot. The study assumed that the ratio of the PCM and base fluids were uniform and stable, and concluded that the overall thermal performance depends on the fusion temperature of the particle. Following Ghalambaz et a. [24], Hajjar et al. [5] investigated the unsteady heat transfer of NEPCMs in a cavity and found a better heat transfer in the presence of NEPCM particles. The results demonstrated that a 2.5% raise of NEPCM volume fraction could enhance the heat transfer by 21%.

The literature review shows that there are only a few studies, which investigated the free convection heat transfer of NEPCM in a porous medium. Ghalambaz et al. [25] modelled the mixed convection boundary-layer heat transfer of NEPCM-suspensions over a flat plate. The outcomes showed the benefit of using NEPCMs on the improvement of the heat transfer, and the fusion temperature of the particles is an essential parameter for heat transfer enhancement. In another study, Ghalambaz et al. [6] addressed the free convection heat transfer of NEPCM-suspensions in a porous cavity and reported that the porosity of the medium is an essential parameter for heat transfer enhancement of NEPCMs. A porous medium with high

porosity is beneficial for using NEPCMs, mainly when the volume fraction of the particles is greater than 3%.

The entropy generation of nanofluids has been investigated in many recent publications. In this regard, Siavashi et al. [26] examined the natural convection entropy generation of nanofluids in a porous fin inside a cavity and found that the thermal irreversibilities were the dominant source of entropy generation in a cavity, and the presence of the porous fins reduced the entropy generation. Shahsavar et al. [27] investigated the free convection heat transfer of hybrid nanofluids (water-Fe3O4/CNT) in an annulus enclosure and reported that using the hybrid nanoparticles intensified both of thermal and friction entropy generations in the enclosure. Different features of entropy generation of nanoliquids have been addressed in recent years, for instance, mass transfer of nanoparticles [28, 29], conjugate heat transfer [30-32], and various geometries [31, 33].

The literature review shows that there are very few studies regarding the free convection heat transfer of nano-encapsulated PCMs in a porous cavity [6]. The entropy generation of NEPCMs is a new topic, which has not been addressed yet. The present study aims to address the entropy generation of NEPCMs in a porous medium for the first time.

2. Problem physics

Natural convection heat transfer in a porous medium occupied by a suspension of water and nano-encapsulated phase change particles is analyzed in the current work. The considered geometry is depicted in Fig. 1. This figure shows a 2D enclosure with the size of L^* and two solid vertical walls with the imposed boundary conditions. The two solid rectangular blocks are located at the left and right sides of the enclosure, and the entire cavity walls are well insulated except the lower part of the left solid wall (hot surface) and the upper surface of the right one (cold surface). Consider a packaging system consist of an array of enclosures depicted in Fig. 1. The hot wall and cold walls are the placement location of charging and discharging pipes in the package. The insulated walls represent the symmetric line between packages. In

such a design, the cold and hot pipes for charging and discharging can be maintained with a sufficient distance and simultaneous charging and discharging is also possible.

In the present model, the Forchheimer term was neglected since the flow in the cavity is induced by the natural convection, and the Darcy-Rayleigh number of the study is typically below 1000. Hence, the velocities in the porous medium are comparatively low. As a result, the inertia effects, which lead to the Forchheimer term, are minimal.

The velocities in the solid domain are forced to zero in the modelling of phase change heat transfer where the PCM phase change. The typical method is the enthalpy-porosity approach. In particular, body forces are introduced in momentum equation to constrain the velocity to zero when PCM becomes solid [34]. Another approach is the viscosity-step function approach, with which viscosity is forced to a very high value to force the velocities to zero [35, 36]. In the present study, the nanoparticles are suspended in the liquid, and the core of nanoparticles could be in solid or liquid states. Regardless of the core status of the nanoparticles, they can circulate with the liquid. Hence, their phase change does not directly influence the velocity profiles. As a result, no velocity control approaches such as enthalpy-porosity or viscosity-step function is required in the present model.

For PCM coupled with porous materials, it is common in literature [34-36] to use a local thermal non-equilibrium approach, with which separate equations are solved for fluid (nanoliquid in this case) and solid (porous material in this case) phases. However, when the thermal conductivity of the porous material is poor, the temperature of the porous matrix can approach the temperature of the liquid inside pores, and local thermal equilibrium approach is reasonable. Here it is assumed that the glass ball porous matrix and the nano liquid are in local thermal equilibrium.

Table 1 lists the thermophysical properties of the NEPCMs particles and water. Details about the latent heat and melting point of the core of the particles can be found in [37].

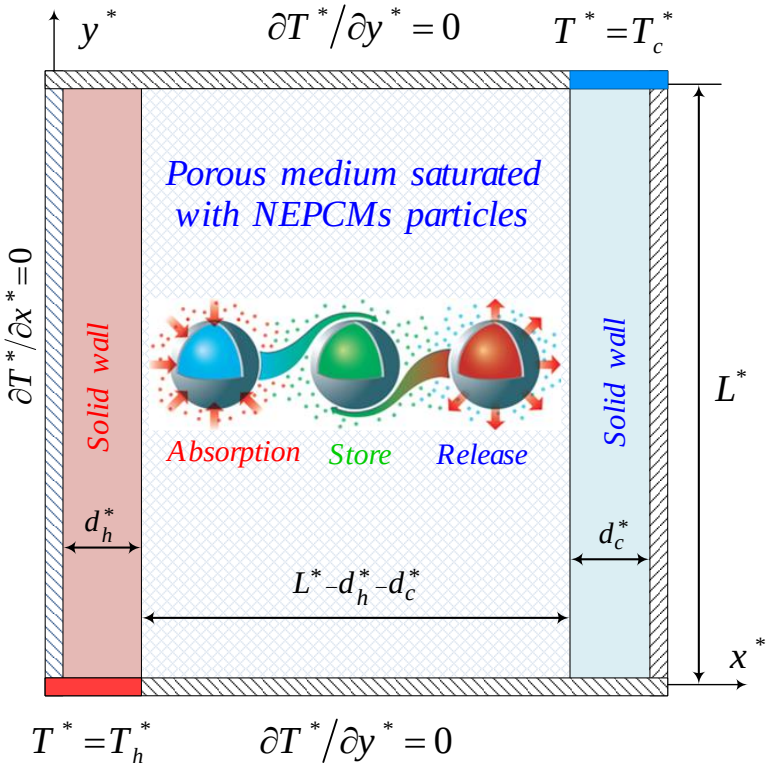

Fig. 1 Schematic configuration of the physical model.

Table 1 Thermophysical properties of the involved materials in the problem [37, 38].

Material	k (Wm^{-1}K^{-1})	ρ (kgm^{-3})	C_p (Jkg^{-1}K^{-1})	β (K^{-1})	μ (kgm^{-1}s^{-1})
Water	0.613	997.1	4179	21×10^{-5}	8.9×10^{-4}
Polyurethane	–	786	1317.7	17.28×10^{-5}	–
Nonadecane	–	721	2037	–	–
Glass balls	1.05	2700	840	0.9×10^{-5}	–

2.1. The formulation

By adopting the Boussinesq's approximation to determine the density variations in an incompressible, laminar and Newtonian nanoliquid inside a porous domain, the governing equations are:

Conservation of mass:

$$\frac{\partial u^*}{\partial x^*} + \frac{\partial v^*}{\partial y^*} = 0 \tag{1}$$

Conservation of momentum:

$$\frac{\rho_b^*}{\varepsilon^2}\left(u^*\frac{\partial u^*}{\partial x^*}+v^*\frac{\partial u^*}{\partial y^*}\right)=-\frac{\partial p^*}{\partial x^*}+\frac{\mu_b^*}{\varepsilon}\left(\frac{\partial^2 u^*}{\partial x^{*2}}+\frac{\partial^2 u^*}{\partial y^{*2}}\right)-\frac{\mu_b^*}{K^*}u^* \tag{2-a}$$

$$\frac{\rho_b^*}{\varepsilon^2}\left(u^*\frac{\partial v^*}{\partial x^*}+v^*\frac{\partial v^*}{\partial y^*}\right)=-\frac{\partial p^*}{\partial y^*}+\frac{\mu_b^*}{\varepsilon}\left(\frac{\partial^2 v^*}{\partial x^{*2}}+\frac{\partial^2 v^*}{\partial y^{*2}}\right)+g^*\rho_b^*\beta_b^*\left(T^*-T_c^*\right)-\frac{\mu_b^*}{K^*}v^* \tag{2-b}$$

Conservation of energy for the porous matrix and the suspension in the pores:

$$\left(\rho^* C_p^*\right)_b\left(u^*\frac{\partial T^*}{\partial x^*}+v^*\frac{\partial T^*}{\partial y^*}\right)=k_{eff}^*\left(\frac{\partial^2 T^*}{\partial x^{*2}}+\frac{\partial^2 T^*}{\partial y^{*2}}\right) \tag{3}$$

In which:

$$k_{eff}^*=(1-\varepsilon)k_s^*+\varepsilon k_b^* \tag{4}$$

Conservation of energy for solid walls:

$$k_w^*\left(\frac{\partial^2 T^*}{\partial x^{*2}}+\frac{\partial^2 T^*}{\partial y^{*2}}\right)=0 \tag{5}$$

Following the physical description of the model in Fig. 1, the boundary conditions at the boundaries of the cavity can be introduced in the following mathematical form:

$$\forall\, x^*,\, y^* \;\middle|\; x^*=0,\ 0\le y^*\le L^* \Rightarrow\ \partial T^*/\partial x^*=0 \tag{6-a}$$

$$\forall\, x^*,\, y^* \;\middle|\; x^*=L^*,\ 0\le y^*\le L^* \Rightarrow\ \partial T^*/\partial x^*=0 \tag{6-b}$$

$$\forall\, x^*,\, y^* \;\middle|\; \begin{array}{l} y^*=0,\ 0\le x^*\le d_h^* \Rightarrow\ T^*=T_h^* \\ y^*=0,\ d_h^*\le x^*\le L^* \Rightarrow\ \partial T^*/\partial y^*=0 \end{array} \tag{6-c}$$

$$\forall\, x^*,\, y^* \;\middle|\; \begin{array}{l} y^*=L^*,\ 0\le x^*\le L^*-d_c^* \Rightarrow\ \partial T^*/\partial y^*=0 \\ y^*=L^*,\ L^*-d_c^*\le x^*\le L^* \Rightarrow\ T^*=T_c^* \end{array} \tag{6-d}$$

$$\forall\, x^*,\, y^* \;\middle|\; \begin{array}{l} x^*=d_h^*,\ 0\le y^*\le L^* \Rightarrow u^*=v^*=0\,, \\ k_w^*\,\partial T^*/\partial y^*\big|_w=k_{eff}^*\,\partial T^*/\partial y^*\big|_b \end{array} \tag{6-e}$$

$$\forall\, x^*,\, y^* \;\left|\begin{array}{l} x^* = L^* - d_c^*,\; 0 \le y^* \le L^* \Rightarrow u^* = v^* = 0\,, \\ k_{eff}^*\; \partial T^* / \partial y^* \big|_b = k_w^*\; \partial T^* / \partial y^* \big|_w \end{array}\right. \tag{6-f}$$

2.2. The suspension thermo-physical properties

The following weighted function of the NEPCMs particles and water gives the density of the nanoliquid [39]:

$$\rho_b^* = (1-\varphi)\,\rho_f^* + \varphi \rho_p^* \tag{7}$$

Densities of water and NEPCMs particles are specified using the *p* and *f* subscripts. The density of the NEPCMs particles is defined based on the densities of its components [39, 40]:

$$\rho_p^* = \frac{(1+\eta)\,\rho_{co}^* \rho_{sh}^*}{\rho_{sh}^* + \eta \rho_{co}^*} \tag{8}$$

where η, i.e. the mass ratio of the core to the shell, is approximately 0.447 [37]. Also, the heat capacity of the nanoliquid is [40, 41]:

$$C_{p,b}^* = \frac{(1-\varphi)\,\rho_f^* C_{p,f}^* + \varphi \rho_p^* C_{p,p}^* \big|_{eff}}{\rho_b^*} \tag{9}$$

$C_{p,p}^* \big|_{eff}$ is the effective heat capacity of the NEPCMs particles and can be obtained using the following relation when there is no the phase change for the core:

$$C_{p,p}^* = \frac{\left(C_{p,co}^* + \eta C_{p,sh}^*\right) \rho_{co}^* \rho_{sh}^*}{\left(\rho_{sh}^* + \eta \rho_{co}^*\right) \rho_p^*} \tag{9}$$

By taking into consideration the phase change of the core of the particles, the heat capacity of the NEPCMs is achieved using a sinusoidal profile as follows [21, 39]:

$$C_{p,p}^{*}\Big|_{eff} = C_{p,p}^{*} + \left\{\frac{\pi}{2}\cdot\left(\frac{h_{sf}^{*}}{T_{Mr}^{*}} - C_{p,p}^{*}\right)\cdot\sin\left(\pi\frac{T^{*}-T_{0}^{*}}{T_{Mr}^{*}}\right)\right\}\times\begin{cases}0 & T^{*}<T_{0}^{*}\\ 1 & T_{0}^{*}<T^{*}<T_{1}^{*}\\ 0 & T^{*}>T_{1}^{*}\end{cases} \quad (10)$$

Since $C_{p,p}^{*}$ is very small compared to h_{sf}^{*}/T_{Mr}^{*}, the term of $\pi C_{p,p}^{*}/2$ can be easily ignored. T_{Mr}, the melting temperature window, is:

$$T_{Mr}^{*} = T_{1}^{*} - T_{0}^{*} \;\Big|\; \begin{matrix} T_{0}^{*} = T_{fu}^{*} - T_{Mr}^{*}/2 \\ T_{1}^{*} = T_{fu}^{*} + T_{Mr}^{*}/2 \end{matrix} \quad (11)$$

in which T_{fu}^{*} is the fusion (melting) temperature of the cores of nano-sized particles. The effective coefficient of the thermal volume expansion for the suspension is written as [41]:

$$\beta_{b}^{*} = (1-\varphi)\beta_{f}^{*} + \varphi\beta_{p}^{*} \quad (12)$$

The dynamic viscosity and thermal conductivity of the suspension are evaluated by utilizing the linear relations presented below [42, 43]:

$$\frac{\mu_{b}^{*}}{\mu_{f}^{*}} = 1 + Nv\varphi \quad (13\text{-a})$$

$$\frac{k_{b}^{*}}{k_{f}^{*}} = 1 + Nc\varphi \quad (13\text{-b})$$

2.3. Stream function and Entropy generation

Streamlines are conveniently employed to depict the fluid flow. For the two-dimensional flow of the suspension comprising NEPCMs, stream function can be obtained as

$$u^{*} = \frac{\partial\Psi^{*}}{\partial y^{*}},\; v^{*} = -\frac{\partial\Psi^{*}}{\partial x^{*}} \quad (14)$$

The above equations can be merged into a single equation as follows:

$$\frac{\partial^2 \Psi^*}{\partial x^{*2}} + \frac{\partial^2 \Psi^*}{\partial y^{*2}} = -\left(\frac{\partial v^*}{\partial x^*} - \frac{\partial u^*}{\partial y^*} \right) \tag{15}$$

and $\Psi^* = 0$ can be considered on all solid boundaries. The produced entropy can be dimensionally calculated as follows [44, 45]:

$$\begin{aligned} S^*_{gen} = {} & \frac{k^*_w}{T^{*2}_0}\left[\left(\frac{\partial T}{\partial x^*} \right)^2 + \left(\frac{\partial T}{\partial y^*} \right)^2 \right] + \frac{k^*_{eff}}{T^{*2}_0}\left[\left(\frac{\partial T}{\partial x^*} \right)^2 + \left(\frac{\partial T}{\partial y^*} \right)^2 \right] \\ & + \frac{\mu^*_b}{T^*_0}\left[\frac{1}{K}(u^{*2} + v^{*2}) + 2\left(\frac{\partial u^*}{\partial x^*} \right)^2 + 2\left(\frac{\partial v^*}{\partial y^*} \right)^2 + \left(\frac{\partial u^*}{\partial y^*} + \frac{\partial v^*}{\partial x^*} \right)^2 \right] \end{aligned} \tag{16}$$

In which the first term indicates the entropy generation due to the heat transfer in the solid walls, the second term characterizes the generated entropy caused by the heat transfer in the fluid and the porous medium, and the last one represents the fluid flow irreversibilities. Moreover, T^*_0 is the average temperature of the cold and hot walls.

3. Non-dimensional governing equations and entropy generation

3.1. Non-dimensional form of governing equations

The dimensionless form of the model equations, Eqs. (1)–(4), and the imposed boundary conditions, Eq. (6), could be obtained by employing the following definitions:

$$\begin{aligned} & x = \frac{x^*}{L^*},\ y = \frac{y^*}{L^*},\ d_h = \frac{d^*_h}{L^*},\ d_c = \frac{d^*_c}{L^*},\ u = \frac{u^* L^*}{\alpha^*_f}, v = \frac{v^* L^*}{\alpha^*_f},\ \Delta T^* = T^*_h - T^*_c \\ & p = \frac{p^* L^{*2}}{\rho^*_f \alpha^{*2}_f},\quad \Psi = \frac{\Psi^*}{\alpha^*_f},\ T = \frac{T^* - T^*_c}{\Delta T^*},\ S = \frac{S^* T^{*2}_0 L^{*2}}{k^*_f \Delta T^*} \end{aligned} \tag{17}$$

Therefore, we then have:

$$\frac{\partial u}{\partial x} + \frac{\partial v}{\partial y} = 0 \tag{18}$$

$$\varepsilon^{-2}\left(\frac{\rho_b}{\rho_f}\right)\left(u\frac{\partial u}{\partial x}+v\frac{\partial u}{\partial y}\right)=-\frac{\partial p}{\partial x}+Pr\,\varepsilon^{-1}\left(\frac{\mu_b}{\mu_f}\right)\left(\frac{\partial^2 u}{\partial x^2}+\frac{\partial^2 u}{\partial y^2}\right)$$
$$-\frac{Pr}{Da}\left(1+Nv\,\phi\right)u \tag{19}$$

$$\varepsilon^{-2}\left(\frac{\rho_b}{\rho_f}\right)\left(u\frac{\partial v}{\partial x}+v\frac{\partial v}{\partial y}\right)=-\frac{\partial p}{\partial y}+Pr\,\varepsilon^{-1}\left(\frac{\mu_b}{\mu_f}\right)\left(\frac{\partial^2 v}{\partial x^2}+\frac{\partial^2 v}{\partial y^2}\right)$$
$$-\frac{Pr}{Da}\left(1+Nv\,\phi\right)v+Ra\cdot Pr\left(\frac{\rho_b}{\rho_f}\right)\left(\frac{\beta_b}{\beta_f}\right)T \tag{20}$$

$$Cr\left(u\frac{\partial T}{\partial x}+v\frac{\partial T}{\partial y}\right)=k_r\left(\frac{\partial^2 T}{\partial x^2}+\frac{\partial^2 T}{\partial y^2}\right) \tag{21}$$

where the Rayleigh (*Ra*), the Prandtl (*Pr*) and the Darcy numbers, are:

$$Ra=\frac{\beta_f^*\,g^*\Delta T^*L^{*3}}{\nu_f^*\alpha_f^*},\ Pr=\frac{\nu_f^*}{\alpha_f^*},\ Da=\frac{K}{L^{*2}} \tag{22}$$

and the heat capacity ratio is:

$$Cr=\frac{\left(\rho^*C_p^*\right)_b}{\left(\rho^*C_p^*\right)_f}=\left(1-\varphi\right)+\varphi\lambda+\frac{\varphi}{\delta\,Ste}f \tag{23}$$

$$k_r=\frac{k_{eff}^*}{k_f^*}=\left(1-\varepsilon\right)\left(\frac{k_s^*}{k_f^*}\right)+\varepsilon\left(1+Nc\,\varphi\right) \tag{24}$$

where *Cr* indicates the ratio of heat capacity of the nanoliquid to the base fluid's sensible heat capacity. Also, the ratio of the heat capacity of the NEPCMs particles to the base fluid (ξ), the melting temperature window in the non-dimensional form (δ), and the Stefan number (*Ste*) are:

$$\xi=\frac{\left(C_{p,co}^*+\eta C_{p,sh}^*\right)\rho_{co}^*\rho_{sh}^*}{\left(\rho^*C_p^*\right)_f\left(\rho_{sh}^*+\eta\rho_{co}^*\right)},\ \delta=\frac{T_{Mr}^*}{\Delta T^*},\ Ste=\frac{\Delta T^*\left(\rho_{sh}^*+\eta\rho_{co}^*\right)\left(\rho^*C_p^*\right)_f}{\left(h_{sf}^*\rho_{co}^*\rho_{sh}^*\right)\left(1+\eta\right)} \tag{25}$$

the non-dimensional fusion function (*f*) was selected as [24]:

$$f = \frac{\pi}{2}\sin\left(\frac{\pi}{\delta}\left(T - T_{fu} + \frac{\delta}{2}\right)\right) \times \begin{cases} 0 & T < T_{fu} - \delta/2 \\ 1 & T_{fu} - \delta/2 < T < T_{fu} + \delta/2 \\ 0 & T > T_{fu} + \delta/2 \end{cases} \quad (26)$$

where T_{fu}, the dimensionless fusion temperature, is.

$$T_{fu} = \frac{T_{fu}^{*} - T_{c}^{*}}{\Delta T^{*}} \quad (27)$$

The energy equation for the solid block is:

$$0 = R_k \left(\frac{\partial^2 T}{\partial x^2} + \frac{\partial^2 T}{\partial y^2}\right) \quad (28)$$

Where $R_k = k_w^* / k_f^*$. Eventually, the normalized boundary constraints are:

$$\forall\, x,\, y \;|\; x = 0,\; 0 \le y \le 1 \Rightarrow\; \partial T/\partial x = 0 \quad (29\text{-a})$$

$$\forall\, x,\, y \;|\; x = 1,\; 0 \le y \le 1 \Rightarrow\; \partial T/\partial x = 0 \quad (29\text{-b})$$

$$\forall\, x,\, y \;\left|\; \begin{array}{l} y = 0,\; 0 \le x \le d_h \Rightarrow\; T = T_h \\ y = 0,\; d_h \le x \le 1 \Rightarrow\; \partial T/\partial y = 0 \end{array}\right. \quad (29\text{-c})$$

$$\forall\, x,\, y \;\left|\; \begin{array}{l} y = 1,\; 0 \le x \le 1 - d_h \Rightarrow\; \partial T/\partial y = 0 \\ y = 1,\; 1 - d_h \le x \le 1 \Rightarrow\; T = T_c \end{array}\right. \quad (29\text{-c})$$

$$\forall\, x,\, y \;\left|\; \begin{array}{l} x = d_h,\; 0 \le y \le 1 \Rightarrow u = v = 0\,, \\ \partial T/\partial y\big|_w = \left[(1-\varepsilon)\left(k_s^*/k_w^*\right) + \varepsilon\left(k_b^*/k_w^*\right)\right]\partial T/\partial y\big|_b \end{array}\right. \quad (29\text{-d})$$

$$\forall\, x,\, y \;\left|\; \begin{array}{l} x = L - d_h,\; 0 \le y \le 1 \Rightarrow u = v = 0\,, \\ \left[(1-\varepsilon)\left(k_s^*/k_w^*\right) + \varepsilon\left(k_b^*/k_w^*\right)\right]\partial T/\partial y\big|_b = \partial T/\partial y\big|_w \end{array}\right. \quad (29\text{-d})$$

3.2. The rate of heat transfer, entropy generation, and the Bejan number

The total entropy generation can be expressed in the dimensionless form as

$$S_{gen} = S_{Th} + S_{Viscous} \quad (30)$$

wherein the S_{Th} and S_{Viscos} are the entropy generation resulted from the heat transfer irreversibility and the frictional force irreversibility, respectively and can be are defined as:

$$S_{Th} = R_k \left[\left(\frac{\partial \theta}{\partial x} \right)^2 + \left(\frac{\partial \theta}{\partial y} \right)^2 \right] + k_r \left[\left(\frac{\partial \theta}{\partial x} \right)^2 + \left(\frac{\partial \theta}{\partial y} \right)^2 \right] \tag{31}$$

$$S_{Viscous} = \Theta . (1 + Nv\,\varphi) \left[\frac{1}{Da} (u^2 + v^2) + 2 \left(\frac{\partial u}{\partial x} \right)^2 + 2 \left(\frac{\partial v}{\partial y} \right)^2 + \left(\frac{\partial u}{\partial y} + \frac{\partial v}{\partial y} \right)^2 \right] \tag{32}$$

Where Θ is the irreversibility parameter:

$$\Theta = \frac{\mu_f^* T_0^*}{k_f^*} \left(\frac{\alpha_f^*}{L^* \Delta T^*} \right)^2 \tag{33}$$

The local and average Bejan numbers are defined as the local and average ratio of heat transfer irreversibility to the total entropy generation over the domain as:

$$Be = \frac{S_{Th}}{S_{gen}}, \qquad Be_{avg} = \frac{\int_A S_{Th} dA}{\int_A S_{gen} dA} \tag{34}$$

It is worth mentioning that *Be* > 0.5 specifies the dominance of heat transfer irreversibility, and *Be* < 0.5 indicates that the irreversibility of fluid friction has prevailed. Concerning the rate of heat transfer, the parameter of interest is the energy transfer from the hot element as:

$$q\left(x^*\right) = -Ak_w \left. \frac{\partial T^*}{\partial y^*} \right)_{y^*=0 \;\&\; 0 \le x^* \le d_h^*} \tag{35}$$

where using the non-dimensional parameters it can be written as:

$$Q\left(x\right) = -R_k \left. \frac{\partial T}{\partial y} \right)_{y=0 \;\&\; 0 \le x \le d_h} \tag{36}$$

The total heat transfer at the wall can be obtained by integration over the length of the wall as:

$$Q_t = \frac{1}{d_h} \int_0^{d_h} Q\left(x\right) dx \tag{37}$$

4. Numerical approach, grid check, and code verification for a further analysis

The equations of the simulated problem are solved by applying the Galerkin Finite Element Method (FEM). The computational domain is discretized by employing a non-uniform structured grid shown in Fig.

2. Besides, to fully couple the discretized equations, the damped Newton method is implemented. The Parallel Sparse Direct Solver is used to find the solution of the obtained linear algebraic equations. Finally, the stopping criteria for the residuals for all dependent variables are considered to be 10^{-5}. More detail about the numerical approach can be found in [46]. Comprehensive grid check has been performed for the employed non-uniform structured grid. The total rate of heat transfer and the maximum value of the streamline are evaluated for five different cases with various grid densities. The studied parameters and the details of the utilized grid are presented in Table 2. As seen, for all of the studied cases, the total rate of heat transfer and the maximum value of the streamlines are approximately constant and not sensible to the utilized grid. Hence, the profile of the fluid temperature for a vertical path at the middle of the cavity, i.e., (X = 0.5), is plotted in Fig. 3 for various grid sizes. Based on the results, the grid with 5180 elements (case 3) is adopted for the simulations.

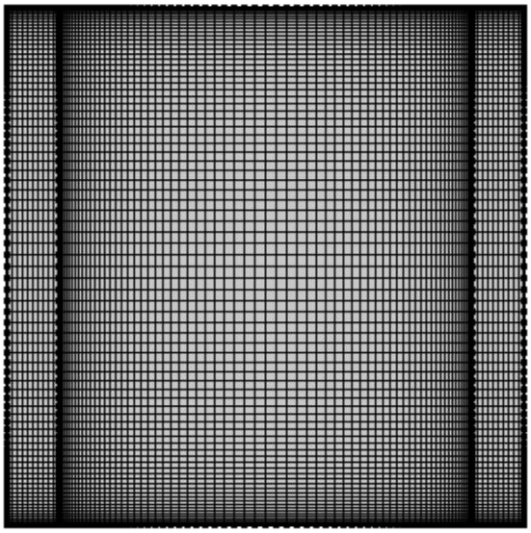

Fig. 2 View of the utilized grid (Case 3)

Table 2 Dependency of the total heat transfer and the flow strength to the grid size (Ra =10^5, R_k =100, Da =10^{-1}, φ = 0.05, Ste = T_{fu} = ε = 0.5, d_s = 0.1).

Case No.	No. of Domain (Boundary) Elements	Q_t	*Err* (%)	$\lvert \Psi_{max} \rvert$	*Err* (%)
1	2300 (292)	38.5941	–	10.5829	–
2	3600 (360)	38.5927	0.0036	10.5878	0.0463
3	5180 (428)	38.5951	0.0025	10.5904	0.0708
4	7200 (500)	38.5968	0.0069	10.5921	0.0869
5	9360 (568)	38.5981	0.0103	10.5931	0.0963

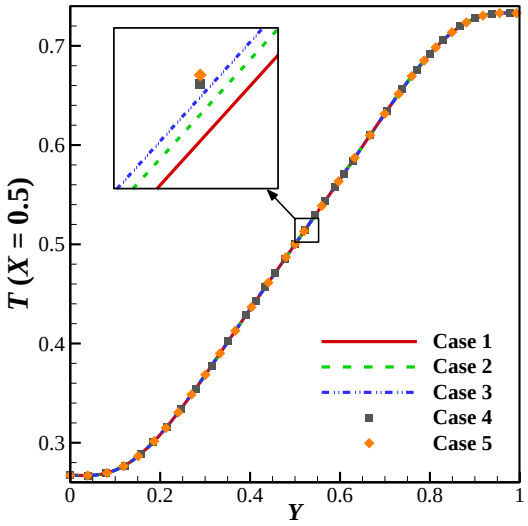

Fig. 3 Temperature the nanoliquid at the middle of the enclosure (X = 0.5) along Y for various mesh sizes.

The current numerical work is verified against three previously published studies. Firstly, the outcomes of this work are verified with the work of Kahveci [47]. Kahveci [47] studied the buoyancy-driven flow inside a clear square cavity with two isothermal cold and hot sidewalls and two adiabatic ones, filled by a nanoliquid. An excellent matching between the heat transfer rates of the present work and those of Kahveci can be found as tabulated in Table 3. Table 4 displays the heat transfer rates of the numerical simulation of this work and that of Nithiarasu et al. [48] for a pure fluid flowing in a porous medium enclosed. The geometry and imposed boundary conditions of Nithiarasu et al. [48] are exactly the same as those taken by [47]. The comparisons between our results and results of Nithiarasu et al. [48] are conducted for different values of *Ra*, *Da*, and ε, showing admissible agreement. Heat transfer and fluid friction components of the entropy generation of the present study have been compared with those reported by Llis et al. [49]. As

displayed in Fig. 4, this evolution specifies the accuracy and correctness of the flow and thermal fields and therefore, the components of entropy generation.

Finally, the outcomes of the developed code are compared against the results of the experimental study of Corvaro and Paroncini [50] on natural convection heat transfer in an air-filled square cavity with a rectangular aluminium heater, in which a 2D-PIV system was used for fluid flow visualization. In [50], the tested enclosure has a dimension of 0.05 m, and with the cold walls of 291.16 K. It is worth noting that the hot wall temperature was changed in order to obtain different values of the Rayleigh number. The width and the height of the hot strip are l = 0.01m and h = 0.025m, respectively and the experiments were conducted for three positions of the aluminum strip, i.e., d = 0.01, 0.015 and 0.02.

Table 3 The comparison of the average Nusselt numbers for the current work and Kahveci [47] when Ra=10^5.

φ	**0.0**	**0.05**	**0.1**	**0.15**
Present study	4.722	4.970	5.191	5.385
Kahveci [47]	4.720	4.970	5.190	5.380

Table 4 The average Nusselt of this work and work of Nithiarasu et al. [48].

ε	Ra	Da	**Present study**	**Reference [48]**
0.4	10^7	10^{-4}	7.77	7.81
0.9	10^7	10^{-4}	9.322	9.202
0.4	10^5	10^{-2}	2.994	2.983
0.9	10^5	10^{-2}	3.92	3.91

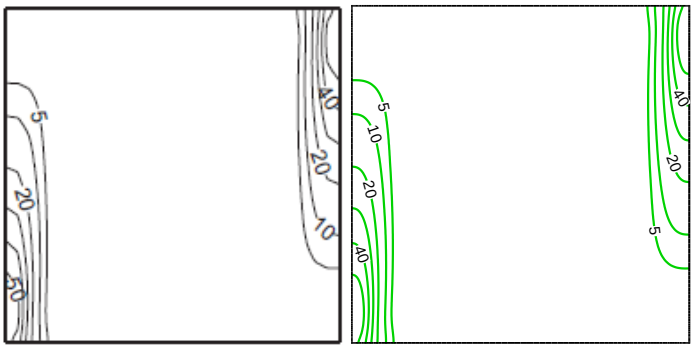

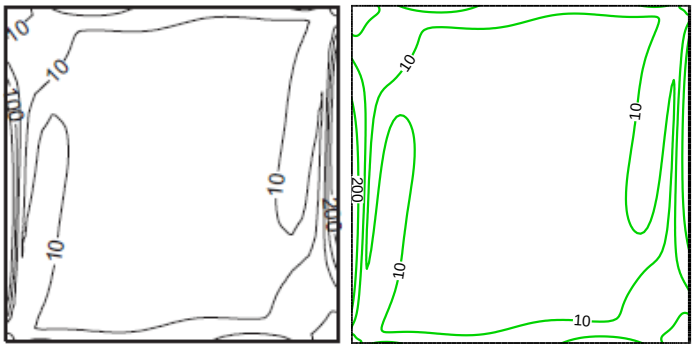

Fig. 4 (a): Entropy generation of thermal gradient and (b): entropy generation of viscosity, work of Llis et al. [49] (left) and present study (right).

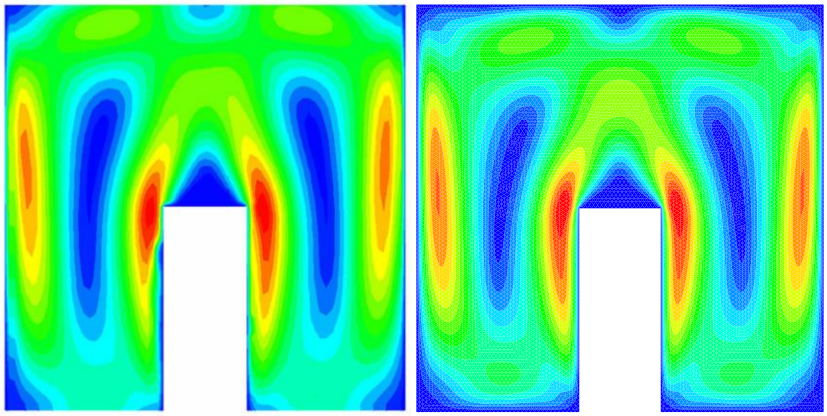

Fig. 5 Comparison between the velocity magnitude obtained by Corvaro and Paroncini [50] (left) and the present study (right) for Pr = 0.71, Ra = 3.16×10^5, d = 0.4.

5. Results and discussion

In this section, the numerical results describing the hydrodynamic and thermal patterns of the nanoliquid containing the NEPCMs particles are presented, and the effect of the following parameters are studied on the fluid flow, entropy generation and heat transfer: Thermal conductivity ratio ($1 \le R_k \le 100$), Darcy number ($10^{-5} \le Da \le 10^{-1}$), porosity ($0.2 \le \varepsilon \le 0.9$), Stefan number ($0.2 \le Ste \le 1$), fusion temperature ($0.05 \le T_{fu} \le 0.95$), solid walls thickness (d_s = 0.1 and 0.3), and the nanoparticle's volume fraction ($0.0 \le \varphi \le 5\%$). The constant parameters are $Ra = 10^5$, Pr = 6.2, Nc = 23.8, Nv = 12.5, k_s/k_f = 1.713 (glass ball to water ratio), and ξ = 0.322.

Influence of the thermal conductivity ratio and the volume fraction of the nano-encapsulated phase change materials on the patterns of streamlines, isotherms of the fluid, local Bejan number and the suspension's heat capacity ratio are outlined in Fig. 6. The stored heat in the capsules during the phase

change is reflected in the suspension's heat capacity, and thus, the green ribbon represents the area, in which the phase change occurs in the capsules. The heat capacity ratio is identical to 0.966 (Eq. 24) when there no phase change occurs. Moreover, *Cr* will surge to its highest value, where the fluid temperature is precisely equal to the fusion temperature of the nano-capsules (4.012 for $Ste = 0.5$ and $\varphi = 0.05$).

Moreover, the green ribbons coincide with the corresponding isothermal lines. Increasing the volume fraction of the NEPCMs raises the viscosity of the suspension and thus slightly reduces the flow strength inside the cavity. In addition, by adding the nano-capsules to the base fluid, the latent heat of the NEPCMs is employed. As the temperature of the suspension remains constant during the phase change (i.e., on the green ribbon), the exerted buoyancy force is reduced, resulting in a slight decline of the fluid strength. Owing to the fluid flow reduction, the isotherms move away from the sidewalls indicating a decline in the nanoliquid temperature gradient.

It is worth mentioning that the thermal conductivity of the suspension, according to Eq. (25), elevates with the increment of the volume fraction of the NEPCMs, and therefore, the total rate of heat transfer intensifies. The contour of the local Bejan number for the case of pure fluid shows that the share of heat transfer in the total irreversibility is mainly in the corners and centre of the cavity, where the velocity gradients are almost negligible. It should be noted that the Be number is identical to unity throughout the solid walls. Adding nano-capsules of the PCM to the host fluid increases the Bejan number in the vicinity of the walls (compare the levels of $Be = 0.5$) as the presence of the NEPCMs boosts the rate of heat transfer. In addition to this, the local Bejan numbers are distorted in the green ribbon, where the capsules undergo a phase transition. Decreasing the solid blocks thermal conductivity reduces the fluid flow and heat transfer in the cavity as it decreases the diffusion of heat through the solid walls. Consequently, a much thicker ribbon is formed.

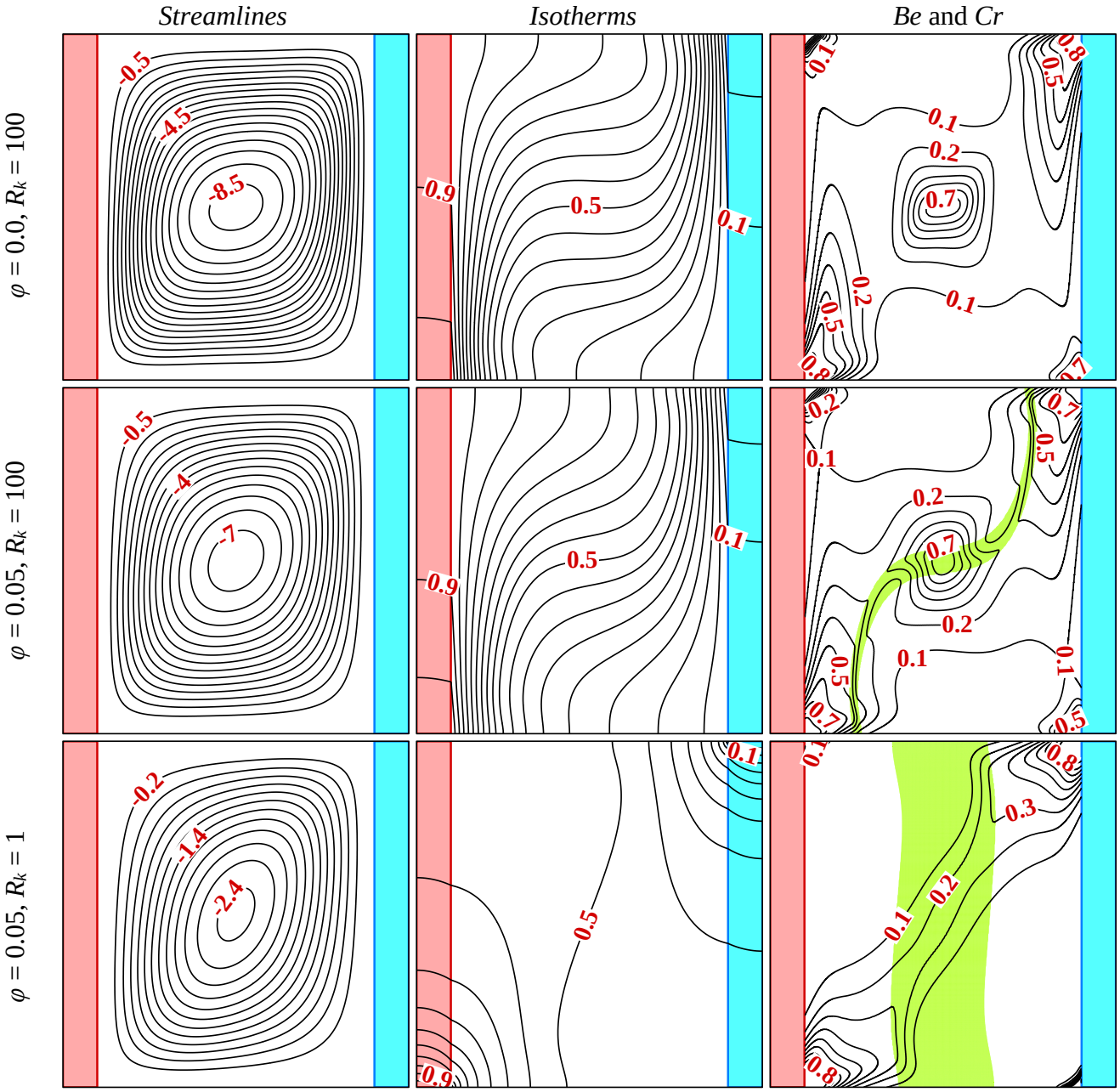

Fig. 6 Variation of the streamlines, isothermal lines, local Bejan number and the heat capacity ratio with the Walls' thickness and the nanoliquid volume fraction ($Da = 10^{-2}$, $Ste = T_{fu} = \varepsilon = 0.5$, $d_s = 0.1$).

Fig. 7 depicts the effect of the porosity of the porous medium and the Darcy number on the streamlines, isothermal lines, local Bejan number, and the heat capacity ratio. The Darcy number indicates the non-dimensional permeability of the medium. For low values of the Darcy number, the fluid strength is low, and the isotherms are almost vertical, specifying that the heat is mainly transferred by conduction mechanism. As a result, the contour of the local Bejan number is approximately symmetric and varies between 0.8 and 1.0, indicating that the heat transfer irreversibilities are dominant throughout the cavity.

Increasing permeability of the solid matrix boosts the fluid flow and thus amplifies the irreversibilities caused by the fluid friction. Increasing porosity, from one hand, reduces the resistance against the fluid flow in the cavity and thus intensifies the convection share of heat transfer. On the other side, by increasing the porosity of the porous medium, according to Eq. (4), the effective thermal conductivity of the suspension and the porous medium declines, and thus, the conduction share of heat transfer decreases. For the set of studied parameters, the overall rate of heat transfer increases since the rate of increase in the convection mode is more than the reduction rate of conduction heat transfer.

Regarding the local values of the Bejan number, it should be noted that increasing porosity reduces the resistance against the fluid flow in the cavity and thus intensifies the fluid strength. Consequently, the irreversibilities induced by the friction of the fluid ($S_{Viscous}$) increases. Moreover, according to the increment of the rate of transferred heat, the heat transfer share of irreversibilities (S_{Th}) will also increase. The average Bejan number is the ratio of the heat transfer irreversibility to the total entropy generation (Eq. 34) and varies between 0 and 1. The overall values of the Bejan isoline decrease as with increasing the porosity of the solid matrix, indicating that the rate of increase in the entropy generation caused by heat transfer (S_{Th}) is much lower than the increment rate of fluid friction entropy generation ($S_{Viscous}$).

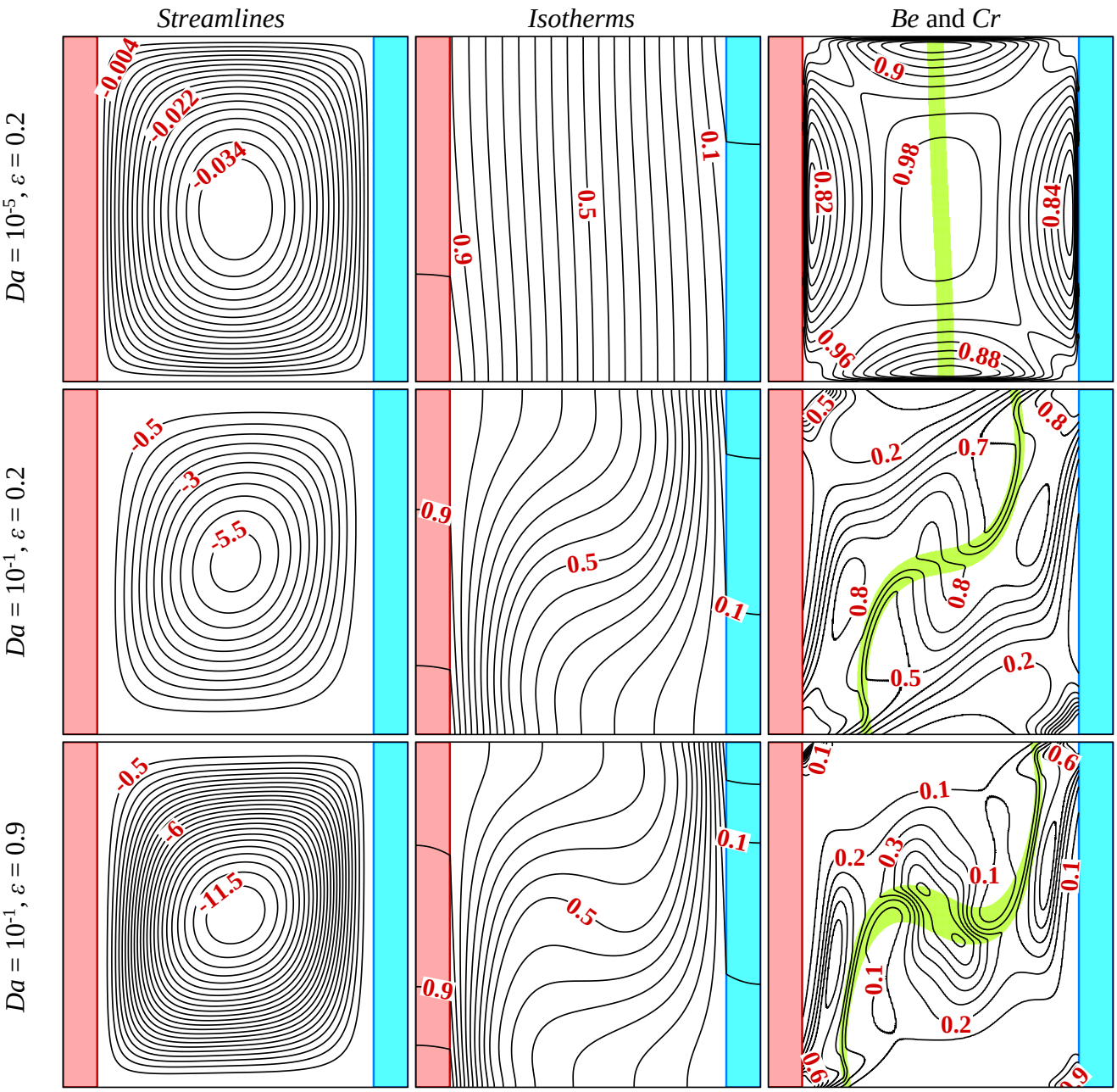

Fig. 7 Variation of the streamlines, isothermal lines, local Bejan number and the heat capacity ratio with Darcy number and porosity of the solid matrix (R_k = 100, φ = 0.05, $Ste = T_{fu}$ = 0.5, d_s = 0.1).

The impact of the dimensionless fusion temperature on the streamlines, isothermal lines, Bejan numbers and the suspension's heat capacity ratio is presented in Fig. 8. As discussed before, the presence of the nano-encapsulated PCMs in the host fluid declines the fluid flow circulation, and this reduction is more pronounced when T_{fu} = 0.5. This can be explained by the fact that the average value of the heat capacity ratio for T_{fu} = 0.5, according to Table 5, is maximum. This means that the phase transition takes place in more nano-sized capsules and therefore the temperature of the suspension is constant in a larger

area, which results in a lower buoyancy force than the other cases of T_{fu} = 0.2 and 0.8. The patterns of the Bejan number exhibit a slight increase when T_{fu} = 0.5, indicating the augmentation of irreversibilities caused by the heat transfer. Furthermore, the isolines of the Bejan number are somewhat distorted within the green ribbon, where the phase change occurs, specifying a sudden change in local irreversibilities.

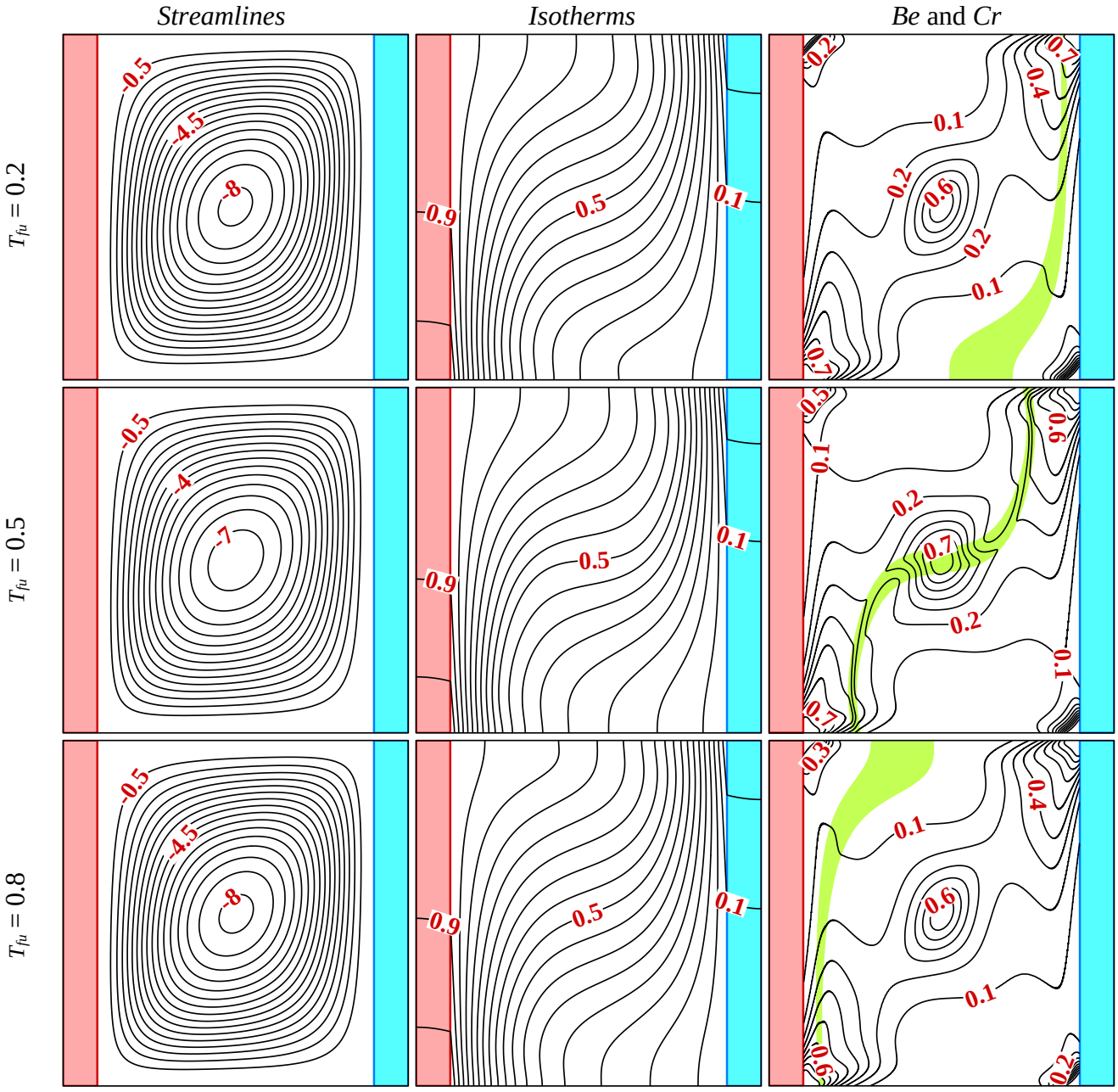

Fig. 8 Variation of the streamlines, isothermal lines, local Bejan number and the heat capacity ratio with dimensionless fusion temperature (Da = 10^{-2}, R_k =100, φ = 0.05, Ste = ε = 0.5, d_s = 0.1).

The dependency of the total heat transfer to the dimensionless fusion temperature, solid walls' thickness, Stefan number and thermal conductivity of the solid walls is depicted in Fig. 9. It is evident that

the graph of heat transfer for each case is symmetric with respect to non-dimensional fusion temperature and reaches its maximum when T_{fu} is the average of the hot and cold walls. In fact, when the fusion temperature approaches its middle value (i.e., 0.5), a higher number of the nano-capsules experience the phase transition and consequently, excessive latent heat is absorbed and released in the cavity, resulting in a higher rate of heat transfer from the hot wall to its cold counterpart. The Stefan number specifies the reciprocal of the capsulated PCMs' non-sensible heat. Therefore, a higher rate of heat transfer is achievable for lower values of the *Ste*, and the influence of the NEPCMs on heat transfer diminishes when it approaches infinity.

Moreover, the total heat transfer for the cases of R_k = 1 and 100 are plotted on separate axes to compare the sensitivity of the Q_t on the fusion temperature. As seen, for the case of R_k = 1, even slight changes of the T_{fu} amplifies the rate of transferred heat; however, for high values of the solid walls' thermal conductivity, the Q_t is almost constant within the ranges of $0.05 \leq T_{fu} \leq 0.25$ and $0.75 \leq T_{fu} \leq 0.95$ (for both cases of d_s = 0.1 and 0.3). Furthermore, increasing the solid walls' thickness reduces the rate of heat transfer for both cases of R_k = 1 and 100. This is plausible as the aspect ratio of the cavity for the fluid flow increases, which subsequently reduces the convection share of heat transfer.

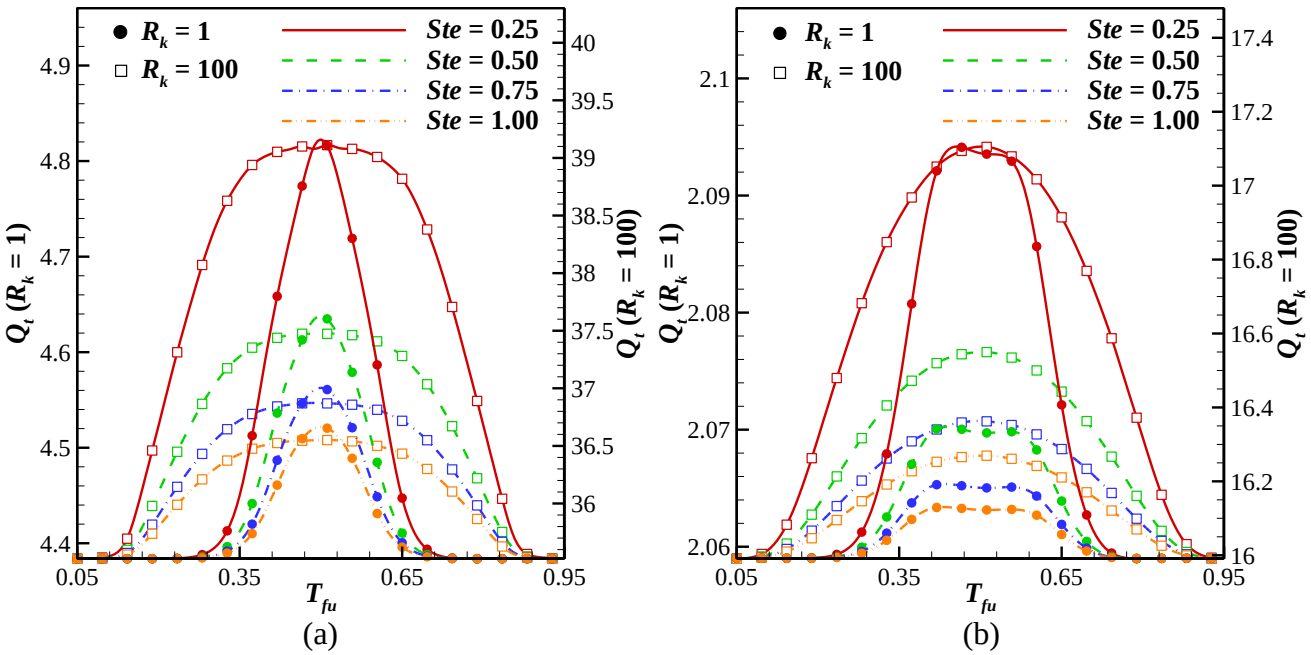

Fig. 9 Variation of the total heat transfer with the non-dimensional fusion temperature, solid walls to fluid thermal conductivity ratio (R_k) and the solid walls thickness (Da = 10^{-2}, φ = 0.05, ε = 0.5) (a) d_s = 0.1 (b) d_s = 0.3.

The influence of the previously discussed parameters on the average Bejan number and the total entropy generation is outlined in Fig. 10. It is noticeable that the extremum values of the average Bejan number and the total entropy generation occur when the fusion temperature equals the average of hot and cold walls temperature (T_{fu} = 0.5). This can be reasoned by considering that when the NEPCMs is added to the base fluid (water), the transferred heat intensifies and the flow strength declines and thus affect the Be_{avg} and S_{gen}. In fact, for d_s = 0.1, the intensification of heat transfer irreversibilities is lower than the reduced rate of irreversibilities caused by fluid friction and thus, while the overall produced entropy decreases the average Bejan number augments.

In addition, increasing the Stefan number lessens the generation of entropy as it decreases the proportion of heat transfer irreversibilities in the enclosure and consequently causes a reduction in the average Bejan number. In contrast with the case of d_s = 0.1, the fluid behavior changes by increasing the thickness of the solid blocks, as shown in Fig. 10b (R_k = 1) and the generated entropy increases and the Bejan number decreases when the fusion temperature approaches 0.5. To analyze this behavior more precisely, the impact of the d_s and R_k on the different parameters are presented in Table 5. When d_s = 0.3,

the flow strength decreases and in contrast with the other cases, the fluid flow increases slightly for T_{fu} = 0.5, which can be explained by the fact that the solid blocks mainly control the heat transfer and the fluid flow. As a result, the produced entropy increased and on the other hand, the average Bejan number decreased when T_{fu} approached 0.5.

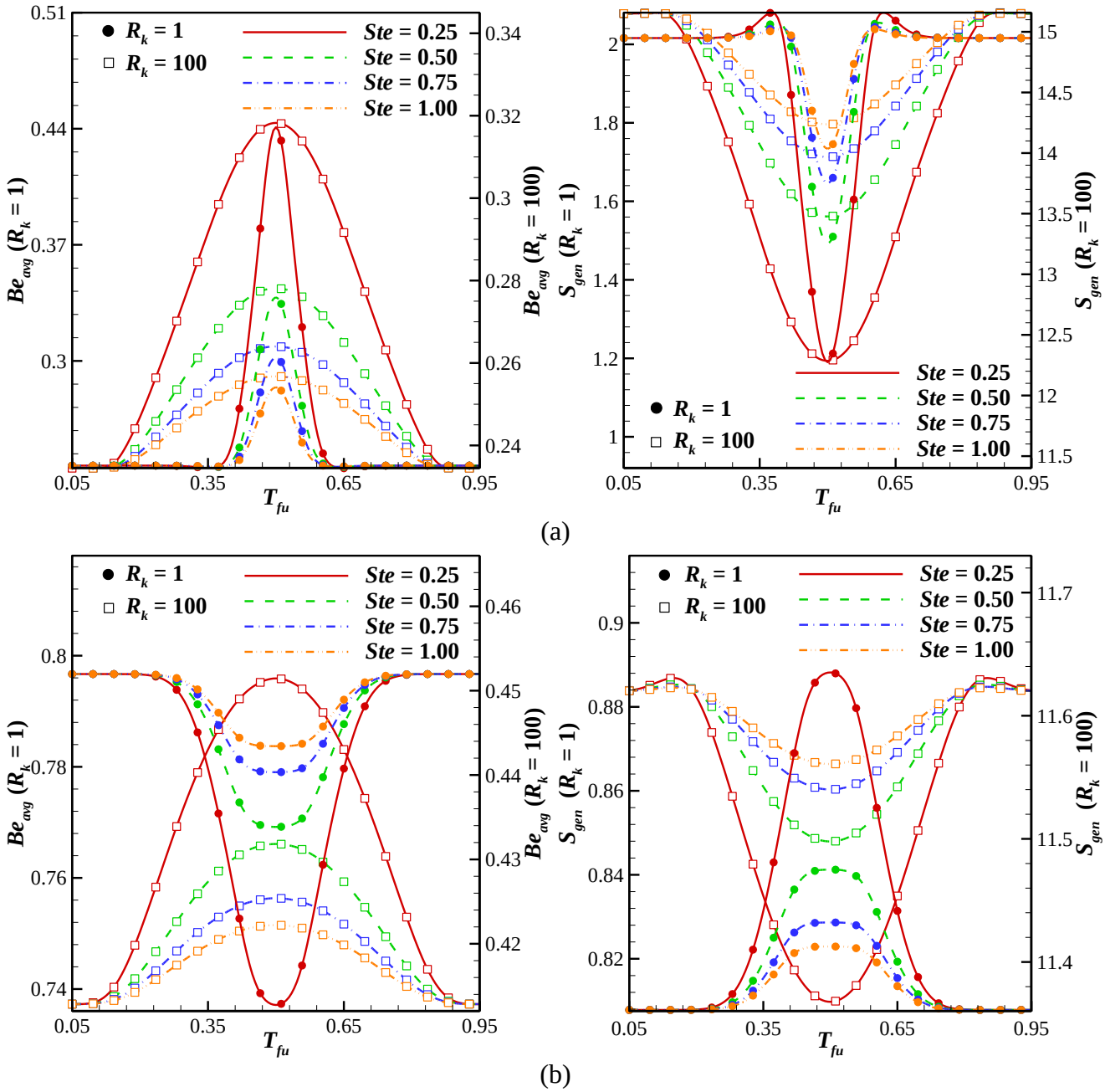

Fig. 10 Dependency of the average Bejan number (left) and total entropy generation (right) to the dimensionless fusion temperature, solid block walls to fluid thermal conductivity ratio (R_k) and the solid walls thickness (Da = 10^2, φ = 0.05, ε = 0.5) (a) d_s = 0.1 (b) d_s = 0.3.

Table 5 Influence of the thickness and thermal conductivity of the solid blocks as well as the dimensionless fusion temperature on the flow and thermal fields and components of the generated entropy ($Da = 10^{-2}$, $\varphi = 0.05$, $\varepsilon = 0.5$).

d_s	R_k	T_{fu}	$\lvert\Psi_{max}\rvert$	Q_t	$\iint CrdA$	S_{gen}	S_{Th}	$S_{Viscous}$	Be_{avg}
0.1	1	0.1	3.2341	4.3838	0.9664	2.0159	0.4775	1.5384	0.2369
		0.5	2.4617	4.6381	1.5816	1.4915	0.5053	0.9863	0.3388
		0.9	3.2341	4.3838	0.9664	2.0159	0.4775	1.5384	0.2369
	100	0.1	8.2178	35.527	0.9986	15.153	3.5530	11.599	0.2345
		0.5	7.2715	37.477	1.0947	13.475	3.7480	9.7271	0.2781
		0.9	8.2178	35.528	0.9986	15.153	3.5530	11.599	0.2345
0.3	1	0.1	0.5076	2.0590	0.9672	0.8078	0.6436	0.1642	0.7967
		0.5	0.5566	2.0697	1.2359	0.8412	0.6471	0.1942	0.7692
		0.9	0.5076	2.0590	0.9672	0.8078	0.6436	0.1642	0.7967
	100	0.1	3.6233	15.998	1.0845	11.623	4.7997	6.8230	0.4129
		0.5	3.5571	16.550	1.0701	11.498	4.9653	6.5326	0.4318
		0.9	3.6233	15.998	1.0845	11.623	4.7997	6.8230	0.4129

Fig. 11 shows the influence of the Darcy number, solid walls' thickness, and the volume fraction of the NEPCMs on the total rate of heat transfer. As discussed before, adding nano-sized capsules to the base fluid boosts the suspension's thermal conductivity and thus intensifies the rate of heat transfer. In addition to this, by increasing the Darcy number, the fluid flow increases, which leads to an augmentation of convection share of the transferred heat. On the other hand, increasing the solid walls boosts the conduction proportion of heat transfer and thus raise the Q_t.

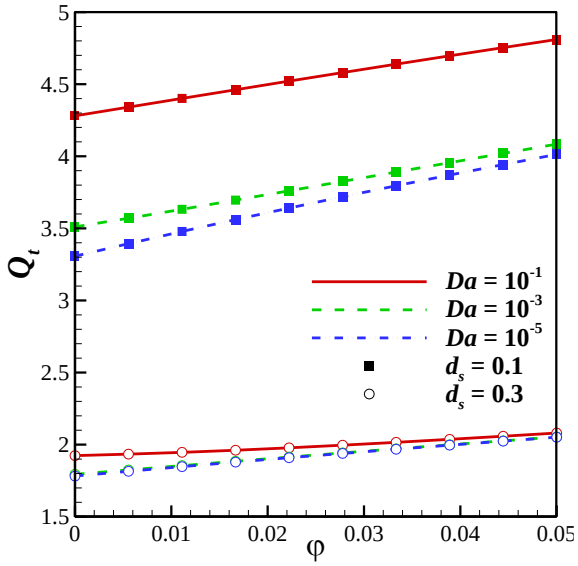

Fig. 11 Variation of the total heat transfer with the Darcy number, solid walls' thickness and volume fraction of the nano-capsules ($Da = 10^{-2}$, R_k =100, $\varepsilon = Ste = 0.5$, $T_{fu} = 0.1$).

The impact of previously discussed parameters on the total rate of produced irreversibilities and the average Bejan number is outlined in Fig. 12. The Bejan number increases continuously with the volume fraction of NEPCMs and the thickness of the solid walls, as they lead to the amplification of the total heat transfer, and decreases with the augmentation of the permeability of the porous matrix as it raises the fluid flow (the denominator of the Eq. 33). On the other hand, the generated entropy shows different trends with increasing the Darcy number. For low values of the Darcy number, the total entropy generation increases with rising the volume fraction of the NEPCMs; however, a downward trend can be found for higher values of the *Da*. This can be explained by the fact that the addition of NEPCMs particles to the base fluid (water), on the one hand, increases the total heat transfer; and, on the other hand, increases the viscosity of the suspension and thus reduces the fluid flow. For low values of the *Da*, the rate of increase in the heat transfer irreversibilities is higher than the reduction rate of friction irreversibilities, and thus, the entropy generation amplifies when φ increases. On the contrary, the reduction of friction-induced irreversibilities overtakes the heat transfer irreversibilities for high values of the Darcy number.

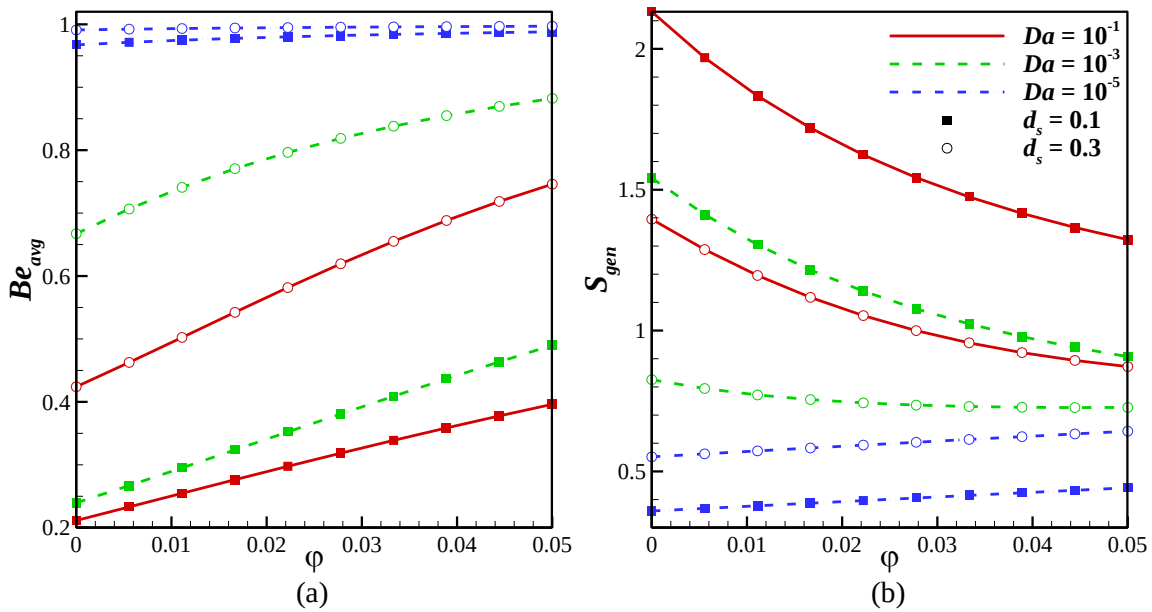

Fig. 12 Influence of the solid walls' thickness, Darcy number and the nano-capsules' volume fraction (Da = 10^{-2}, R_k =100, ε = Ste = 0.5, T_{fu} = 0.1) on the (a) Be_{avg} and (b) S_{gen}.

6. Conclusion

The present study comprehensively analyzed the entropy generation and convective heat transfer of a suspension comprising NCPCM materials in a porous square cavity. Steady-state 2-dimensional conjugate free convection of an aqueous suspension containing NEPCMs was analyzed inside a porous square cavity with two solid blocks. The cores of the discussed nano-sized capsules were filled with the Nonadecane, and their shell was made from polyurethane (PU). The released latent heat of the nonadecanes during the phase change process of the capsules was reflected in the nanoliquid local heat capacity. Thus, the heat capacity field varies with the temperature of the nanoliquid. The non-linear coupled governing equations, including the continuity, *x*- and *y*-momentum equations for the suspension and the energy equations for the fluid and solid walls were first non-dimensionalized and then solved using the Galerkin finite element method. Influence of various non-dimensional parameters such as the Darcy number, porosity of the solid matrix, volume fraction of the NEPCMs, thermal conductivity and thickness of the solid walls, dimensionless fusion temperature and the Stefan number were addressed on the fluid flow, rate of heat transfer and the suspension's entropy generation. The key findings could be summarized as follows:

- Increasing the volume fraction of the NEPCMs raises the viscosity of the suspension and thus slightly reduces the flow strength inside the cavity;

- The fluid flow and heat transfer in the cavity amplify with the increment of the thermal conductivity ratio as it boosts the diffusion of heat through the solid walls;
- For low values of the solid matrix permeability, the contour of local Bejan number is approximately symmetric and varies between 0.8 and 1.0, indicating that the heat transfer irreversibilities is dominant throughout the cavity;
- The highest heat transfer rate can be accomplished when the fusion temperature of the nano-capsules is $T_{fu} = 0.5$. Moreover, for $d_s = 0.1$, the heat transfer can be increased up to 10% when $T_{fu} \approx 0.5$. In addition, the total heat transfer rate decreases with the increment of the Stefan number as well as the augmentation of the solid walls' thickness;
- For low values of the solid walls' thickness, the extremum values of the total rate of entropy generation and average Bejan number occur when the dimensionless fusion temperature equals the average of hot and cold walls temperature ($T_{fu} = 0.5$);
- Increasing the Stefan number lessens the generation of entropy as it decreases the proportion of heat transfer irreversibilities in the enclosure and consequently causes a reduction in the average Bejan number;
- Addition of 5% volume fraction of nano-capsules (when $T_{fu} = 0.1$) to water can boost the rate of heat transfer up to 12.3% for $d_s = 0.1$ and 8.3% for $d_s = 0.3$;
- For high values of the solid wall's thickness, a reverse trend can be observed when its thermal conductivity is low ($R_k = 1$), and the generated entropy increases and the Bejan number decreases when the fusion temperature approaches 0.5;
- Increment of the Darcy number enhances the fluid strength and leads to an augmentation of convection share of the transferred heat;
- The average Bejan number elevates by the increment of the NEPCMs' volume fraction since is intensifies the rate of heat transfer. Moreover, Be_{avg} decreases with augmentation of the permeability of the porous matrix as it increases the fluid strength;

- For low values of the Darcy number, the total entropy generation increases with rising the volume fraction of the NEPCMs; however, a downward trend can be found for higher values of the *Da*.
- The average Bejan number increases up to 87% and the total entropy generation decreases to about 61% when 5% of nano-capsules is added to water (T_{fu} = 0.1 and d_s = 0.1).

The results of the current work revealed that the Darcy number and the fusion temperature of NEPCM particles were key parameters in controlling the heat transfer and entropy generation for the steady-state thermal enhancement applications. Another aspect of using NEPCMs is the latent heat thermal energy storage. Hence, the investigation of the impact of these key parameters on the transient thermal behaviour of NEPCMs during a charging/discharging thermal cycle could be investigated in future studies.

Conflicts of interest

The authors declare no conflicts of interest.

References

[1] M. Kenisarin, K. Mahkamov, Solar energy storage using phase change materials, Renewable and sustainable energy reviews, 11(9) (2007) 1913-1965.

[2] H. Chen, Y. Ding, T. Peters, F. Berger, Method of Storing Energy and a Cryogenic Energy Storage System, in, Google Patents, 2016.

[3] E. Bonamente, A. Aquino, Environmental Performance of Innovative Ground-Source Heat Pumps with PCM Energy Storage, Energies, 13(1) (2020) 117.

[4] P.B. Salunkhe, P.S. Shembekar, A review on effect of phase change material encapsulation on the thermal performance of a system, Renewable and Sustainable Energy Reviews, 16(8) (2012) 5603-5616.

[5] A. Hajjar, S. Mehryan, M. Ghalambaz, Time periodic natural convection heat transfer in a nano-encapsulated phase-change suspension, International Journal of Mechanical Sciences, 166 (2020) 105243.

[6] M. Ghalambaz, S. Mehryan, A. Hajjar, A. Veisimoradi, Unsteady natural convection flow of a suspension comprising Nano-Encapsulated Phase Change Materials (NEPCMs) in a porous medium, Advanced Powder Technology, (2019).

[7] T. Nomura, N. Okinaka, T. Akiyama, Impregnation of porous material with phase change material for thermal energy storage, Materials Chemistry and Physics, 115(2-3) (2009) 846-850.

[8] R. Hossain, S. Mahmud, A. Dutta, I. Pop, Energy storage system based on nanoparticle-enhanced phase change material inside porous medium, International Journal of Thermal Sciences, 91 (2015) 49-58.

[9] S.A. Memon, H. Cui, T.Y. Lo, Q. Li, Development of structural–functional integrated concrete with macro-encapsulated PCM for thermal energy storage, Applied energy, 150 (2015) 245-257.

[10] X. Xiao, P. Zhang, M. Li, Preparation and thermal characterization of paraffin/metal foam composite phase change material, Applied Energy, 112 (2013) 1357-1366.

[11] Z.A. Qureshi, H.M. Ali, S. Khushnood, Recent advances on thermal conductivity enhancement of phase change materials for energy storage system: A review, International Journal of Heat and Mass Transfer, 127 (2018) 838-856.

[12] Z. Chen, D. Gao, J. Shi, Experimental and numerical study on melting of phase change materials in metal foams at pore scale, International Journal of Heat and Mass Transfer, 72 (2014) 646-655.

[13] M. Iasiello, K. Braimakis, A. Andreozzi, S. Karellas, Thermal analysis of a Phase Change Material for a Solar Organic Rankine Cycle, Journal of Physics: Conference Series, 923 (2017) 012042.

[14] S. Mancin, A. Diani, L. Doretti, K. Hooman, L. Rossetto, Experimental analysis of phase change phenomenon of paraffin waxes embedded in copper foams, International Journal of Thermal Sciences, 90 (2015) 79-89.

[15] H. Cui, W. Tang, Q. Qin, F. Xing, W. Liao, H. Wen, Development of structural-functional integrated energy storage concrete with innovative macro-encapsulated PCM by hollow steel ball, Applied energy, 185 (2017) 107-118.

[16] R. Fukahori, T. Nomura, C. Zhu, N. Sheng, N. Okinaka, T. Akiyama, Macro-encapsulation of metallic phase change material using cylindrical-type ceramic containers for high-temperature thermal energy storage, Applied energy, 170 (2016) 324-328.

[17] T. Toppi, L. Mazzarella, Gypsum based composite materials with micro-encapsulated PCM: Experimental correlations for thermal properties estimation on the basis of the composition, Energy and Buildings, 57 (2013) 227-236.

[18] A. El Ouali, T. El Rhafiki, T. Kousksou, A. Allouhi, M. Mahdaoui, A. Jamil, Y. Zeraouli, Heat transfer within mortar containing micro-encapsulated PCM: Numerical approach, Construction and Building Materials, 210 (2019) 422-433.

[19] L.F. Cabeza, C. Castellon, M. Nogues, M. Medrano, R. Leppers, O. Zubillaga, Use of microencapsulated PCM in concrete walls for energy savings, Energy and Buildings, 39(2) (2007) 113-119.

[20] E. Alehosseini, S.M. Jafari, Micro/nano-encapsulated phase change materials (PCMs) as emerging materials for the food industry, Trends in Food Science & Technology, (2019).

[21] H.R. Seyf, Z. Zhou, H. Ma, Y. Zhang, Three dimensional numerical study of heat-transfer enhancement by nano-encapsulated phase change material slurry in microtube heat sinks with tangential impingement, International journal of heat and mass transfer, 56(1-2) (2013) 561-573.

[22] H. Reza Seyf, M.R. Wilson, Y. Zhang, H. Ma, Flow and heat transfer of nanoencapsulated phase change material slurry past a unconfined square cylinder, Journal of Heat Transfer, 136(5) (2014).

[23] C.-J. Ho, W.-C. Chen, W.-M. Yan, Correlations of heat transfer effectiveness in a minichannel heat sink with water-based suspensions of Al2O3 nanoparticles and/or MEPCM particles, International Journal of Heat and Mass Transfer, 69 (2014) 293-299.

[24] M. Ghalambaz, A.J. Chamkha, D. Wen, Natural convective flow and heat transfer of nano-encapsulated phase change materials (NEPCMs) in a cavity, International Journal of Heat and Mass Transfer, 138 (2019) 738-749.

[25] M. Ghalambaz, T. Groşan, I. Pop, Mixed convection boundary layer flow and heat transfer over a vertical plate embedded in a porous medium filled with a suspension of nano-encapsulated phase change materials, Journal of Molecular Liquids, 293 (2019) 111432.

[26] M. Siavashi, R. Yousofvand, S. Rezanejad, Nanofluid and porous fins effect on natural convection and entropy generation of flow inside a cavity, Advanced Powder Technology, 29(1) (2018) 142-156.

[27] A. Shahsavar, P.T. Sardari, D. Toghraie, Free convection heat transfer and entropy generation analysis of water-Fe3O4/CNT hybrid nanofluid in a concentric annulus, International Journal of Numerical Methods for Heat & Fluid Flow, (2019).

[28] A.I. Alsabery, E. Gedik, A.J. Chamkha, I. Hashim, Impacts of heated rotating inner cylinder and two-phase nanofluid model on entropy generation and mixed convection in a square cavity, Heat and Mass Transfer, 56(1) (2020) 321-338.

[29] A. Alsabery, R. Mohebbi, A. Chamkha, I. Hashim, Impacts of magnetic field and non-homogeneous nanofluid model on convective heat transfer and entropy generation in a cavity with heated trapezoidal body, Journal of Thermal Analysis and Calorimetry, 138(2) (2019) 1371-1394.

[30] M.S. Ishak, A.I. Alsabery, A. Chamkha, I. Hashim, Effect of finite wall thickness on entropy generation and natural convection in a nanofluid-filled partially heated square cavity, International Journal of Numerical Methods for Heat & Fluid Flow, (2019).

[31] T. Tayebi, A.J. Chamkha, Entropy generation analysis during MHD natural convection flow of hybrid nanofluid in a square cavity containing a corrugated conducting block, International Journal of Numerical Methods for Heat & Fluid Flow, (2019).

[32] A.I. Alsabery, M.A. Ismael, A.J. Chamkha, I. Hashim, Impact of finite wavy wall thickness on entropy generation and natural convection of nanofluid in cavity partially filled with non-Darcy porous layer, Neural Computing and Applications, (2020) 1-21.

[33] M. Mansour, T. Armaghani, A. Chamkha, A. Rashad, Entropy generation and nanofluid mixed convection in a C-shaped cavity with heat corner and inclined magnetic field, The European Physical Journal Special Topics, 228(12) (2019) 2619-2645.

[34] W.Q. Li, Z.G. Qu, Y.L. He, W.Q. Tao, Experimental and numerical studies on melting phase change heat transfer in open-cell metallic foams filled with paraffin, Applied Thermal Engineering, 37 (2012) 1-9.

[35] P. Di Giorgio, M. Iasiello, A. Viglione, M. Mameli, S. Filippeschi, P. Di Marco, A. Andreozzi, N. Bianco, Numerical Analysis of a Paraffin/Metal Foam Composite for Thermal Storage, Journal of Physics: Conference Series, 796 (2017) 012032.

[36] Y. Tian, C.Y. Zhao, A numerical investigation of heat transfer in phase change materials (PCMs) embedded in porous metals, Energy, 36(9) (2011) 5539-5546.

[37] S. Barlak, O.N. Sara, A. Karaipekli, S. Yapıcı, Thermal Conductivity and Viscosity of Nanofluids Having Nanoencapsulated Phase Change Material, Nanoscale and Microscale Thermophysical Engineering, 20(2) (2016) 85-96.

[38] M. Ghalambaz, M.A. Sheremet, I. Pop, Free convection in a parallelogrammic porous cavity filled with a nanofluid using Tiwari and Das' nanofluid model, PloS one, 10(5) (2015) e0126486.

[39] L. Chai, R. Shaukat, L. Wang, H.S. Wang, A review on heat transfer and hydrodynamic characteristics of nano/microencapsulated phase change slurry (N/MPCS) in mini/microchannel heat sinks, Applied Thermal Engineering, 135 (2018) 334-349.

[40] B. Chen, X. Wang, R. Zeng, Y. Zhang, X. Wang, J. Niu, Y. Li, H. Di, An experimental study of convective heat transfer with microencapsulated phase change material suspension: laminar flow in a circular tube under constant heat flux, Experimental Thermal and Fluid Science, 32(8) (2008) 1638-1646.

[41] K. Khanafer, K. Vafai, A critical synthesis of thermophysical characteristics of nanofluids, International journal of heat and mass transfer, 54(19-20) (2011) 4410-4428.

[42] A. Zaraki, M. Ghalambaz, A.J. Chamkha, M. Ghalambaz, D. De Rossi, Theoretical analysis of natural convection boundary layer heat and mass transfer of nanofluids: Effects of size, shape and type of nanoparticles, type of base fluid and working temperature, Advanced Powder Technology, 26(3) (2015) 935-946.

[43] M. Ghalambaz, A. Doostani, E. Izadpanahi, A.J. Chamkha, Phase-change heat transfer in a cavity heated from below: The effect of utilizing single or hybrid nanoparticles as additives, Journal of the Taiwan Institute of Chemical Engineers, 72 (2017) 104–115.

[44] T. Basak, A.K. Singh, R. Anandalakshmi, Analysis of Entropy Generation during Conjugate Natural Convection within a Square Cavity with Various Location of Wall Thickness, Industrial & Engineering Chemistry Research, 53(9) (2014) 3702-3722.

[45] A.J. Chamkha, A.M. Rashad, M.A. Mansour, T. Armaghani, M. Ghalambaz, Effects of heat sink and source and entropy generation on MHD mixed convection of a Cu-water nanofluid in a lid-driven square porous enclosure with partial slip, Physics of Fluids, 29(5) (2017) 052001.

[46] J.N. Reddy, An introduction to the finite element method, New York, 1993.

[47] K. Kahveci, Buoyancy driven heat transfer of nanofluids in a tilted enclosure, Journal of Heat Transfer, 132(6) (2010) 062501.

[48] P. Nithiarasu, K. Seetharamu, T. Sundararajan, Natural convective heat transfer in a fluid saturated variable porosity medium, International Journal of Heat and Mass Transfer, 40(16) (1997) 3955-3967.

[49] G.G. Ilis, M. Mobedi, B. Sunden, Effect of aspect ratio on entropy generation in a rectangular cavity with differentially heated vertical walls, International Communications in Heat and Mass Transfer, 35(6) (2008) 696-703.

[50] F. Corvaro, M. Paroncini, An experimental study of natural convection in a differentially heated cavity through a 2D-PIV system, International Journal of Heat and Mass Transfer, 52(1) (2009) 355-365.